IOPscience iopscience.iop.org

Home Search Collections Journals About Contact us My IOPscience

Design and fabrication of a InGaN vertical-cavity surface-emitting laser with a composition-graded electron-blocking layer

This content has been downloaded from IOPscience. Please scroll down to see the full text.

2014 Laser Phys. Lett. 11 085002

(http://iopscience.iop.org/1612-202X/11/8/085002)

View the table of contents for this issue, or go to the journal homepage for more

Download details:

IP Address: 140.113.38.11
This content was downloaded on 25/12/2014 at 02:30

Please note that terms and conditions apply.

IOP Publishing | Astro Ltd Laser Physics Letters
Laser Phys. Lett. **11** (2014) 085002 (5pp) doi:10.1088/1612-2011/11/8/085002

Design and fabrication of a InGaN vertical-cavity surface-emitting laser with a composition-graded electron-blocking layer

B C Lin[1], Y A Chang[2], K J Chen[1], C H Chiu[3], Z Y Li[1], Y P Lan[1], C C Lin[4], P T Lee[1], Y K Kuo[2], M H Shih[5], H C Kuo[1], T C Lu[1] and S C Wang[1]

[1] Department of Photonics & Institute of Electro-Optical Engineering, National Chiao Tung University, Hsinchu 300, Taiwan
[2] Department of Physics, National Changhua University of Education, Changhua 500, Taiwan
[3] Advanced Optoelectronic Technology Inc., Hsinchu 303, Taiwan
[4] Institute of Photonics System, National Chiao Tung University, Tainan 711, Taiwan
[5] Research center for Applied Science, Taipei 115, Taiwan

Email: rayman0313@gmail.com and hckuo@faculty.nctu.edu.tw

Received 30 July 2014
Accepted for publication 8 May 2014
Published 17 June 2014

Abstract

In this study, the design and fabrication of a InGaN vertical-cavity surface-emitting laser (VCSEL) with a composition-graded electron blocking layer (GEBL) are revealed experimentally and theoretically. It has been demonstrated that laser output performance is improved by using a GEBL when compared to the typical VCSEL structure of a rectangular EBL. The output power obtained at 20 kA cm^{-2} is enhanced by a factor of 3.8 by the successful reduction of threshold current density from 12.6 to 9.2 kA cm^{-2} and the enlarged slope efficiency. Numerical simulation results also suggest that the improved laser output performances are due mainly to the reduction of electron leakage current and the enhanced hole injection efficiency in the multiple-quantum-well (MQW) active region.

Keywords: nitride, VCSEL, electron blocking layer

(Some figures may appear in colour only in the online journal)

1. Introduction

Nitride-based materials have attracted much attention due to the large tunable direct band gap and their promising potentials for optoelectronic devices, including high power electronic devices, light-emitting diodes (LEDs), laser diodes (LDs), and VCSELs. High-brightness InGaN/GaN LEDs, based on a double-heterostructure design, were demonstrated by Nakamura *et al* [1]; then the related ultraviolet, blue, and green LEDs were commercialized in the following years [2, 3]. InGaN-based LDs were also realized under room-temperature (RT) continuous-wave (CW) operation by Nakamura *et al* [4, 5]. So far, InGaN-based LDs have been widely used in high-density optical storage systems, laser projection displays, and other applications [6, 7]. In addition, much effort has been devoted to the development of InGaN-based VCSELs, since they are promising in single longitudinal mode emission, light emission in vertical direction, circular beam shape, low divergence angle, lower manufacturing costs, and formation of two-dimensional arrays [8–12]. For InGaN-based VCSELs, the active region conventionally consists of InGaN MQWs and GaN barriers, followed by a *p*-doped AlGaN EBL, which is inevitably used to block the electrons from escaping to the *p*-layers and to maintain the crystalline quality of the active region during the subsequent crystal growth and device processing [13]. However, it has been reported that the large polarization field in AlGaN EBL reduces the effective barrier height for electrons [14]. The overflow of electrons

 © 2014 Astro Ltd Printed in the UK

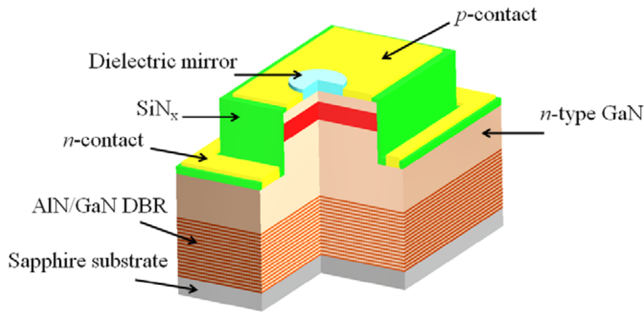

Figure 1. Schematic diagram of the InGaN-based VCSEL structure in this specific study.

outside the active region would recombine with the holes in *p*-layers, which is detrimental to the output performance of laser devices. The polarization-field induced band-bending and the increased potential barrier height nearby the EBL in the valance band also retard the injection of holes. A similar phenomenon has been observed in GaN-based LEDs [15, 16].

Therefore, to solve the aforementioned problems, several alternatives for replacing the AlGaN EBL have been explored, including high-bandgap InAlN, which is lattice-matched to GaN [17], quaternary AlInGaN [18] in InGaN-based LEDs, and step-graded AlGaN [19] in InGaN-based LDs. In our prior study, the feasibility of using GEBL with Al composition increasing along the [0001] direction has been shown numerically in InGaN-based LEDs. Superior LED performance, including high output power and low efficiency droop behavior, has been confirmed evidentially [20]. To further prove the feasibility of using GEBL, we present in this study the design and fabrication of InGaN-based VCSELs with GEBL experimentally. Meanwhile, theoretical explanation of the improved laser performance is given by using an advanced simulator [21].

2. Experiments

The structure of a conventional InGaN-based VCSEL, used as a reference in this study, was prepared grown on a *c*-plane sapphire substrate by a metal-organic chemical vapor deposition (MOCVD) system. The subsequent epitaxial structure consisted of a 30 nm thick GaN nucleation layer, 25 pairs of AlN/GaN distributed Bragg reflectors (DBRs), a 880 nm thick *n*-type GaN layer (*n*-doping = 5×10^{18} cm^{-3}), ten pairs of $In_{0.1}Ga_{0.9}N$ (2.5 nm)/GaN (10 nm) MQWs, followed by a 20 nm thick *p*-$Al_{0.25}Ga_{0.75}N$ EBL (*p*-doping = 3×10^{17} cm^{-3}), and a 100 nm thick *p*-type GaN layer (*p*-doping = 5×10^{17} cm^{-3}). In the fabrication process, a 200 nm thick SiN_x layer was deposited by the plasma-enhanced chemical vapor deposition as a current-confined layer. In this way, the current injection aperture was designed to be about 10 μm in diameter. Then, a 40 nm thick indium-tin-oxide (ITO) layer was deposited as the current spreading layer and annealed at 600 °C for 10 min by rapid thermal annealing. Then, the *p*-contact and *n*-contact were deposited with Ni/Au of about 20 nm/150 nm and Ti/Al/Ni/Au of about 20 nm/150 nm/20 nm/150 nm by the E-gun system, respectively. Finally, ten pairs of Ta_2O_5/SiO_2 of the top dielectric DBRs were deposited by the ion-assisted E-gun system to complete the whole InGaN-based VCSEL devices. Both the 25 pairs AlN/GaN DBR and the ten pairs Ta_2O_5/SiO_2 DBR show a high reflectivity over 99% at the peak wavelength at 410 nm in the *n-k* measurement system. Figure 1 shows the schematic diagram of the InGaN-based VCSEL structure in this specific study. For the VCSEL with GEBL structure design, it is almost identical to the referenced VCSEL structure except that the conventional rectangular AlGaN EBL is replaced by GEBL directly. During the epitaxial growth, the composition in a ternary III-nitride semiconductor can be graded by two methods: growth temperature ramping and III/III ratio ramping [22, 23]. Here we have adopted the Al/Ga ratio ramping because the higher temperature might damage the quality of InGaN MQWs. The growth temperature of conventional EBL and GEBL was kept the same as 870 °C, and the aluminum-composition profile of GEBL was approximately graded from 0% to 25%.

3. Theoretical models and simulation parameters

3.1. Theoretical models

To investigate the effects of using GEBL, and to further analyze the carrier transport and distribution within the MQW active region of the InGaN-based VCSELs, an advanced simulator (Photonic Integrated Circuit Simulator in 3D, PICS3D) is utilized in this specific study. The PICS3D is based on three-dimensional finite element analysis and can deal with the optical and electrical properties of the optoelectronic devices by solving Poisson's equation, current continuity equations, carrier transport equations, complex wave equations, and photon rate equations. The carrier-transport model includes the drift and diffusion of electrons and holes in semiconductors. For VCSELs, the carrier-transport and Poisson equations are solved in cylindrical coordinate system. Built-in polarization induced by spontaneous and piezoelectric polarization is considered at hetero-interfaces of nitride-based devices. In the optical mode model, a basic scalar complex wave equation is solved for the lateral modes, while the effective index method is chosen for the calculation of the optical lateral modes in VCSELs. The method decouples the optical fields in both the vertical and the transverse directions [21].

3.2. Simulation parameters

An important issue in any device simulation is the selection of proper material parameters in the physical models. In this study, the bandgap energies of the $In_xGa_{1-x}N$ and $Al_xGa_{1-x}N$ ternary alloys can be expressed as follows:

$$E_g(In_xGa_{1-x}N) = xE_g(InN) + (1-x)E_g(GaN) - 1.4x(1-x) \quad (1)$$

$$E_g(Al_xGa_{1-x}N) = xE_g(AlN) + (1-x)E_g(GaN) - 0.7x(1-x) \quad (2)$$

where E_g(InN), E_g(AlN), and E_g(GaN) are the bandgap energies of InN, AlN, and GaN, which have values of 0.71, 6.28, and 3.42 eV at 300 K, respectively. The band-offset ratio, which is defined as the ratio between the conduction-band offset ΔE_c and the valance-band offset ΔE_v, is assumed to be 0.7/0.3 for both the InGaN and AlGaN material systems.

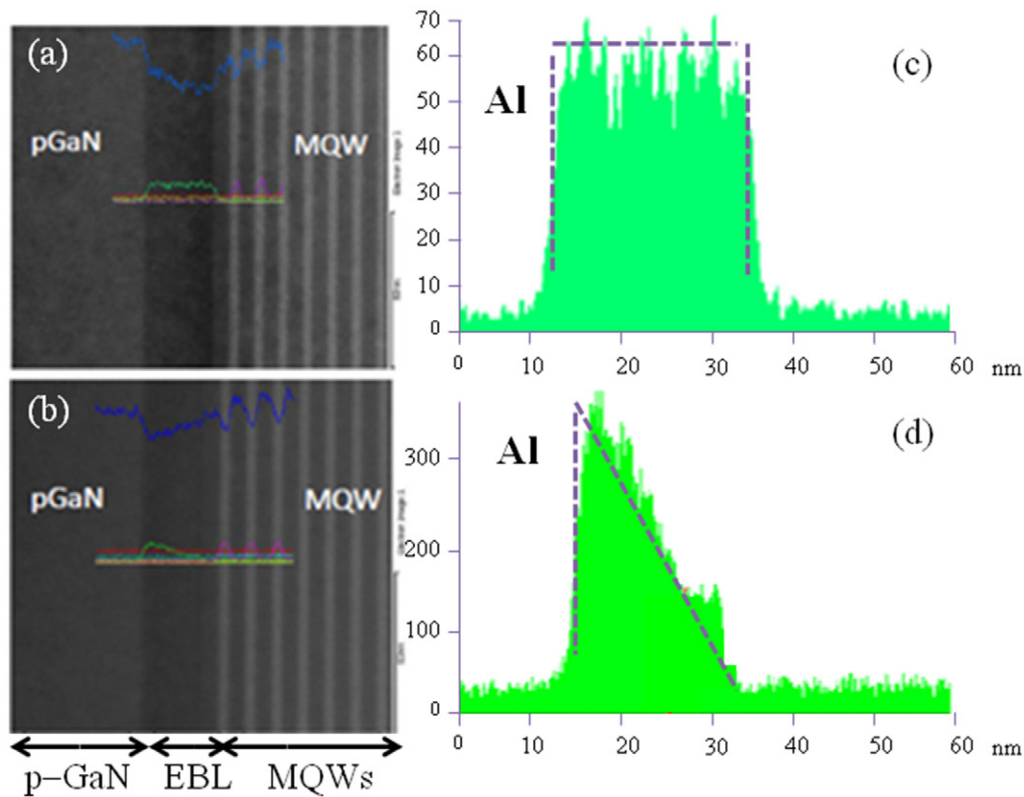

Figure 2. Cross-sectional TEM images nearby the MQW active regions of the VCSELs with (*a*) conventional rectangular $Al_{0.25}Ga_{0.75}N$ EBL and (*b*) GEBL. The EDS curves of (*c*) conventional rectangular $Al_{0.25}Ga_{0.75}N$ EBL and (*d*) GEBL.

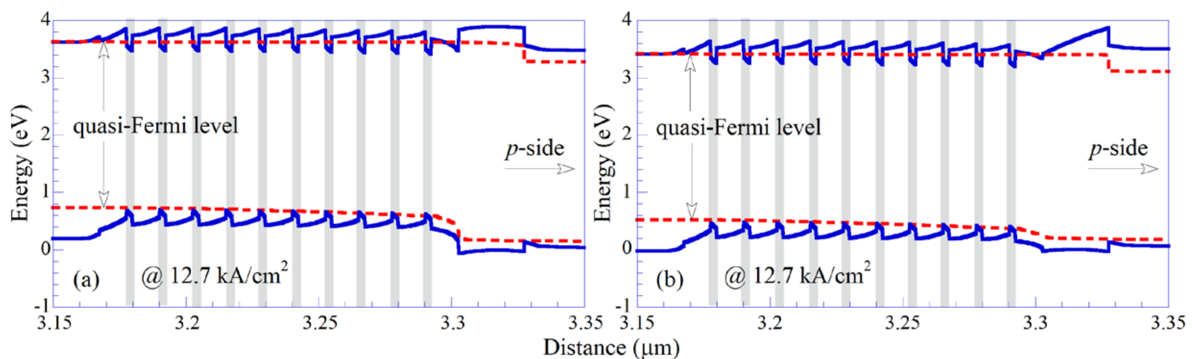

Figure 3. Calculated energy band diagrams near the active regions of the VCSELs with (*a*) conventional rectangular $Al_{0.25}Ga_{0.75}N$ EBL and (*b*) GEBL at a current density of 12.7 kA cm^{-2}.

The nonradiative carrier lifetime is assumed to be 50 ns for InGaN and 1 ns for AlGaN. We use a Mg activation energy of 170 meV for GaN which is assumed to increase by 3 meV per Al% for AlGaN. Built-in polarization induced by spontaneous and piezoelectric polarization is known to influence the performance of InGaN-based VCSELs [24]. In order to consider the built-in polarization within the interfaces of InGaN-based VCSELs, a method developed by Fiorentini *et al* is employed to estimate the built-in polarization, which is represented by fixed interface charges at each hetero-interface [25]. Although the interface charges can be calculated by this theoretical model, the amount of interface charges obtained from experimental measurement is generally varying from 20% to 80% as compared to that obtained from theoretical calculation. It is mainly attributed to the partial compensation of the built-in polarization by both defects inside the device and injected charge carriers. The separation of electrons and holes within the QWs, which are attributable to built-in polarization fields, reduces the photon emission rate and leads to an increased threshold current of the VCSELs. In this study, in order to have the best fitting to the experimental results, the percentage of screening effect is assumed to be 40% of the calculated value in simulations. Other parameters of the semiconductors used in the simulation are referred to in [26].

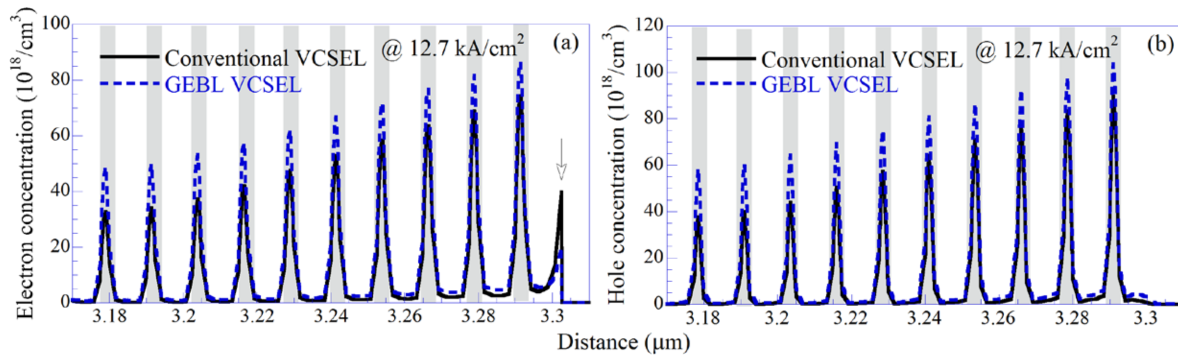

Figure 4. Distribution of (*a*) electron concentration and (*b*) hole concentration near the MQW active region of the VCSELs with conventional rectangular EBL and GEBL at current density of 12.7 kA cm^{-2}.

4. Results and discussion

The morphologies and elemental composition of the VCSELs with conventional rectangular EBL and GEBL examined by transmission electron microscopy (TEM) and energy dispersive spectrometer (EDS) are shown in figures 2(*a*)–(*d*). It is clearly found from the EDS analysis in figure 2(*d*) that the Al composition in GEBL is graded from 0% to 25% approximately. Noteworthily, we still can observe in figure 2(*a*) that there exist several abnormal dark regions at the interface between $Al_{0.25}Ga_{0.75}N$ EBL and the last GaN barrier in the VCSEL structure with conventional rectangular $Al_{0.25}Ga_{0.75}N$ EBL, which indicates that the crystalline quality of the conventional rectangular $Al_{0.25}Ga_{0.75}N$ EBL may not be so good in contrast to the GEBL, as depicted in figure 2(*b*).

In this specific study, the laser output performance of the VCSELs is simulated numerically in advance to provide a qualitative analysis for realizing the fundamental physics of the VCSELs. Figure 3 shows the energy band diagrams near the active regions of the VCSELs with conventional rectangular EBL and GEBL at a current density of 12.7kA cm^{-2}. The gray areas in the figures indicate the locations of QWs. Severe band-bending occurs within the active region i.e. sloped triangular barriers and wells are observed in the active region of the VCSELs, which indicates that the polarization-induced electric field separates the electrons and holes to the opposite sides of the QWs, resulting in the decrease of radiative recombination since the overlap between the electron and hole wave functions is reduced. Figure 3(*a*) shows more clearly that the polarization-induced electric field, which exists at the interface of last-barrier/EBL, bends the band profile of the last barrier downward. Under this circumstance, the effective potential barrier height in the conduction band for confining electrons within the QW active region is reduced. This band-bending will cause an accumulation of electrons and then leads to severe electron leakage [26]. Also, an unwilling barrier arises in the valence band, which makes the holes more difficult to transport into the active region. The corresponding increase in electron leakage and the difficulty in hole injection are expected to have detrimental effects on the VCSELs.

As shown in figure 3(*b*), this obstacle can be easily eliminated by grading the Al composition in AlGaN EBL, since the

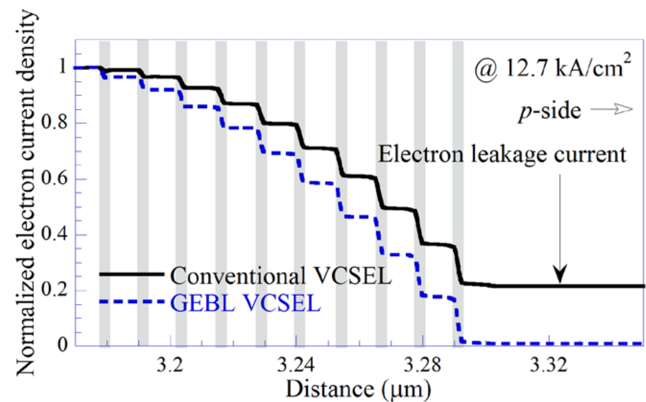

Figure 5. Normalized electron current density flowing along the growth direction near the MQW active region of the VSCELs with conventional rectangular EBL and GEBL at a current density of 12.7 kA cm^{-2}.

polarization charge density at the interface of the last-barrier/EBL can be reduced. This GEBL structure is found evidently to provide a flatter band profile of the last GaN barrier, while the effective potential barrier height in the conduction band to confine electrons can be increased simultaneously. Moreover, it needs to be underscored that the abrupt barrier height, at the interface of the last-barrier/EBL in the valence band when using conventional rectangular EBL, can be reduced. Therefore, the hole injection efficiency can be improved effectively.

Figure 4 shows the distribution of the carrier concentration within the MQW active region of the VCSELs with conventional rectangular EBL and GEBL at a current density of 12.7kA cm^{-2}. It is clearly found in figure 4(*a*) that more electrons can be confined efficiently within the MQW active region when the GEBL structure is utilized. Also, there are more electrons accumulated at the interface of last-barrier/EBL for the VCSEL with conventional rectangular EBL due to severer band banding, which may also induce a more detrimental electron leakage current. As shown in figure 4(*b*), compared to the VCSEL with conventional rectangular EBL, there are more holes distributed within the MQW active region when the GEBL structure is utilized. The hole injection efficiency is improved evidentially. As a result, the radiative recombination can be increased accordingly, since

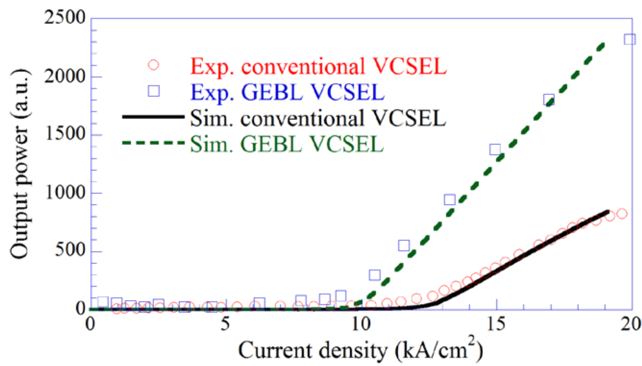

Figure 6. Laser output performances of the VCSELs with conventional rectangular EBL and GEBL obtained by experiment and numerical simulation.

more carriers are accumulated within the MQW active region. Figure 5 shows the normalized electron current density flowing along the growth direction near the MQW active region of the VSCELs with conventional rectangular EBL and GEBL at a current density of 12.7kA cm^{-2}. The electron leakage current density can be suppressed attractively when the GEBL structure is utilized.

Laser output performances of the VCSELs, with conventional rectangular EBL and GEBL obtained by experiment and numerical simulation, are shown in figure 6. The results are obtained at 300 K under CW current injection. Both the results obtained numerically for the VCSELs, with either conventional rectangular EBL or GEBL, are in good agreement with those obtained from experiments. As illustrated in figures 4 and 5, higher recombination efficiency results because more carriers accumulate within the MQW active region; as a result, the threshold current density can be reduced from 12.6 to 9.2 kA cm^{-2} and the slope efficiency can be improved when the GEBL structure is utilized. Accordingly, the laser output power can be increased by a factor of 3.8 when the injection current density is 20 kA cm^{-2}.

5. Conclusion

In summary, laser output performances of the InGaN-based VCSELs have been successfully improved in this study. The results obtained experimentally show that the output power obtained at 20 kA cm^{-2} is enhanced by a factor of 3.8 by the successful reduction of threshold current density from 12.6 to 9.2 kA cm^{-2} and the enlarged slope efficiency when the GEBL structure is utilized. Numerical simulation results also suggest that the improved laser output performances are due mainly to the reduction of electron leakage current and the enhanced hole injection efficiency in the MQW active region. This work suggests that better laser output performances of the InGaN-based VCSELs can be further obtained by the polarization-engineering in the MQW active region.

Acknowledgments

The authors thank Dr. Tien-Chang Lu and Dr. Shing-Chung Wang of National Chiao Tung University for their technical support and discussions. This work was funded by the National Science Council in Taiwan under grants of NSC-103-3113-E-009-001-CC2.

References

[1] Nakamura S, Mukai T and Senoh M 1994 *Appl. Phys. Lett.* **64** 1687–9
[2] Nakamura S, Senoh M, Iwasa N and Nagahama S I 1995 *Japan J. Appl. Phys.* **34** L797–9
[3] Taniyasu Y, Kasu M and Maimoto T 2006 *Nature* **441** 325–8
[4] Nakamura S, Senoh M, Nagahama S I, Iwasa N, Matsushita T and Mukai T 2000 *Appl. Phys. Lett.* **76** 22–4
[5] Nakamura S, Senoh M, Nagahama S I, Iwasa N, Yamada T, Matsushita T, Sugimoto Y and Kiyoku H 1996 *Appl. Phys. Lett.* **69** 4056–8
[6] Ichimura I, Maeda F, Osato K, Yamamoto K and Kasami Y 2000 *Jpn. J. Appl. Phys.* **39** 937–42
[7] Maeda T, Terao M and Shimano T 2003 *Jpn. J. Appl. Phys.* **42** 1044–51
[8] Towe E, Leheny R F and Yang A 2000 *IEEE J. Sel. Topics Quantum Electron.* **6** 1458–64
[9] Iga K 2000 *IEEE J. Sel. Topics Quantum Electron.* **6** 1201–15
[10] Chow W W, Choquette K D, Crawford M H, Lear K L and Hadley G R 1997 *IEEE J. Sel. Topics Quantum Electron.* **10** 1810–24
[11] Lu T C, Kuo C C, Kuo H C, Huang G S and Wang S C 2008 *Appl. Phys. Lett.* **92** 141102
[12] Higuchi Y, Omae K, Matsummura H and Mukai T 2008 *Appl. Phys. Express* **1** 121102
[13] Wu L W *et al* 2003 *IEEE Trans. Electron Devices* **50** 1766
[14] Han S H *et al* 2009 *Appl. Phys. Lett.* **94** 231123
[15] Kim M H, Schubert M F, Dai Q, Kim J K, Schubert E F, Piprek J and Park Y 2007 *Appl. Phys. Lett.* **18** 183507
[16] Han S H 2009 *Appl. Phys. Lett.* **94** 231123
[17] Choi S, Kim H J, Kim S S, Liu J, Kim J, Ryou J H, Dupuis R D, Fischer A M and Ponce F A 2010 *Appl. Phys. Lett.* **96** 221105
[18] Kuo Y K, Tasi M C and Yen S H 2009 *Opt. Commun.* **282** 4252–5
[19] Zhang Y, Kao T T, Liu J, Lochner Z, Kim S S, Ryou J H, Dupuis R D and Shen S C 2011 *J. Appl. Phys.* **109** 083115
[20] Wang C H *et al* 2010 *Appl. Phys. Lett.* **97** 261103
[21] PICS3D 2012 Crosslight Software Inc. (Burnaby, Canada) (www.crosslight.com)
[22] Sun C K, Chiu T L, Keller S, Wang G, Minsky M S, DenBaars S P and Bowers J E 1997 *Appl. Phys. Lett.* **71** 425
[23] Kim M H, Do Y G, Kang H C, Noh D Y and Park S J 2001 *Appl. Phys. Lett.* **79** 2713
[24] Piprek J, Farrell R, DenBaars S and Nakamura S 2006 *IEEE Photon. Technol. Lett.* **18** 7–9
[25] Fiorentini V, Bernardini F and Ambacher O 2002 *Appl. Phys. Lett.* **80** 1204–6
[26] Vurgaftman I and Meyer J R 2003 *J. Appl. Phys.* **94** 3675–96
[27] Chen J R, Lee C H, Ko T S, Chang Y A, Lu T C, Kuo H C, Kuo Y K and S C Wang 2008 *J. Lightwave Technol.* **26** 329–36